Chapter 4

Studies on photocatalytic degradation of MB with Iodine doped TiO_2 nanoparticles

Abstract

In present work, Iodine-doped TiO_2 (IDT) photocatalysts were prepared employing solution-combustion process in various mol % of iodine (I), i.e., $Ti_{1-x}I_xO_2$ (x = 0.00- 0.05). Fourier transform infrared spectroscopy (FTIR), X-ray diffraction (XRD) and UV-Vis Diffuse Reflectance spectroscopic (DRS) were used to characterise the synthesised IDT. DRS indicated that iodine doping increased the absorbance range while diminishing its bandgap energy. As the I doping concentration in TiO_2 increased, there was a constant shift in absorbance towards the visible light area. The XRD demonstrated that the prepared photocatalysts were solely with the anatase phase of TiO_2. The FTIR identified the functional groups in the prepared photocatalysts and numerous Ti-O lattice stretching and bending vibrational bands. Photocatalytic degradation of methylene blue (MB) dye was tested in a UV photochemical reactor. The 3% IDT photocatalyst has the highest photodegradation efficiency amid all the prepared pristine and IDT photocatalysts. Regarding dye photodegradation, the synthesized TiO_2 photocatalyst doped with 3% Iodine outperformed the commercially available Aeroxide P-25 photocatalyst. Furthermore, the prepared photocatalysts demonstrated excellent reusability in regeneration trials. A study on the germination of "*Vigna Radiata*" was done to determine phytotoxicity as part of the investigation into the potential use of photocatalytically treated water in irrigation. The phytotoxicity evaluation results show that the treated water has potential for use in irrigation.

4.1 Introduction:

This work focuses on synthesising pristine and Iodine-doped TiO_2 (IDT) nanoparticles utilising cost-effective TiO_2 powder. The synthesis process involves a solution combustion method using citric acid as a fuel and subsequent calcination to enhance the crystallinity. This method creates fine TiO_2 particles by limiting their growth, which is easy and cheap. The degradation of the MB dye in the UV Photochemical reactor served as the basis for investigating the photocatalytic performance of the photocatalysts. The influence of several variables, including pH, catalyst dose and initial dye concentration, were studied for their optimization. Also, the regeneration and phytotoxicity study has been performed. The Table 4.1 mentions a brief of studies related to I doped TiO_2's use in degradation of various pollutants.

Table 4.1 Previous Literature related to I doped TiO_2

S.N.	Dopant Level	Pollutant	Intial conc.	Results	Ref.
1.	7% mole	Rhodamine B	20 ppm	92.85% degradation in 3h under sunlight	[1]
2.	3% mole	Direct blue-199	300 ppm	Under UV and visible light	[2]
3.	15% mole	Acid Orange 7 (AO7)	20 ppm	100% degradation in 3h under visible light irradiation.	[3]
4.	0.3% wt.	Acetone	400 ppm	94% degradation in 5h under visible light irradiation.	[4]
5.	10% wt.	CO_2	200 ppm	under visible light irradiation.	[5]
6.	0.5% mole	Bisphenol A	10 ppm	86% degradation in 66.5 min under visible light irradiation and 100% under sunlight.	[6]

4.2 Materials and Methods

4.2.1 Chemicals used

The Chemicals used in this study were Titanium (IV) oxide (TiO_2) powder of purity 99%, Iodic acid (HIO_3), Ammonium sulphate ($(NH_4)_2SO_4$), Sulphuric acid (H_2SO_4) 98% concentrated, Liquid ammonia 25% concentrated (sp. gr. 0.91), Citric acid monohydrate ($C_6H_8O_7.H_2O$), and Nitric acid (HNO_3) 70% concentrated and methylene blue (MB) dye. These materials were bought from Merck, India.

4.2.2 Preparation of IDT nanoparticles:

TiO_2 nanoparticles were prepared by solution-combustion synthesis. The stoichiometric amount of TiO_2 was dissolved in 100 mL of H_2SO_4 with ammonium sulphate in a beaker. The ratio of TiO_2 and $(NH_4)_2SO_4$ was 1:6 by mole. Again, the stoichiometric amount of iodic acid was taken in separate beaker and dissolved in 50 mL of H_2SO_4. These solutions were heated on a hot plate with a magnetic stirrer for 3 h at 170 °C. Subsequently, both solutions were mixed and further diluted with distilled water to 500 mL. The solution was cooled at ambient temperature and neutralised by ammonia solution dropwise until the formation of a white precipitate. The formed residue was collected using a Buchner funnel and dissolved in 50 mL of nitric acid. Citric acid monohydrate of about 10 g was added and stirred. The solution was evaporated at 80 °C while continuously stirring until self-ignition occurred. Self-ignition took place at room temperature; due to this, many gases were released, and a fluffy mass (brown) was formed, which was then pulverised into fine particles with a pestle and mortar. During the ignition process, citric acid formed a complex with cations, providing fuel for combustion. The ignition phase elevated the temperature, resulting in the formation of crystalline powder. This powder was then placed in an electrical furnace for calcination at 500°C for 5 h to get the final IDT nanoparticles. One of the key reasons for using monohydrate citric acid is its

environmental friendliness and ease of degradation. Citric acid belongs to the group of organic acids that are easier to degrade and are considered more environmentally friendly than some synthetic chelating agents like EDTA and DPTA [7].

4.2.3 Characterisations:

XRD analysis was used to identify the phases of the prepared IDT photocatalysts and the average crystallite size conducted by Cu K irradiation (Ultima IV; Rigaku, Japan). XPS analysis (AMICUS, Kratos Analytical, UK) was used to estimate the binding energy of the elements in the samples using a monochromated Mg K (1253.6 eV) X-ray source. With barium sulphate used as an internal reference, the UV-Vis absorption spectra of the prepared IDT photocatalysts were examined by DRS (CORY 100 Bio UV spectrophotometer). The Kubelka-Munk technique was used to determine the indirect bandgap energy of the IDT photocatalysts by plotting $[F(R)\times h]^{1/2}$ vs the photon energy (hv). The IR spectra were recorded using the KBr pellet method with the Nicholet 5700 (Thermo Electron) FTIR spectrophotometer. The photocatalytic activity was evaluated for all prepared and regenerated photocatalysts by recording MB concentration reduction with time, i.e., by knowing the kinetics of the photocatalytic reaction.

4.2.4 Methodology of the kinetic study:

The dye degradation kinetics was studied using a UV-PCR reactor equipped with a quartz tube. Different concentrations of aqueous dye solutions, precisely 10 ppm, 20 ppm, 30 ppm, 40 ppm, and 50 ppm, were employed in the experiments. Using this quartz tube, a 100 mL dye solution with 0.01g photocatalyst was kept in a UV-PCR reactor for kinetic analysis. After inserting a magnetic bar, the stirring and UV lamp were turned on. A 2 mL sample was collected every 5 min, centrifuged for 2 min, and then their dye concentration

was determined. This method was also used to study dye kinetics with other synthesised nanoparticles in a UV-PCR reactor.

The photocatalytic activity of both the pristine and regenerated 3% IDT photocatalysts was studied in a UV-PCR reactor using 30 ppm dye concentration. The degradation kinetics of the dye solution was studied to estimate photocatalytic activity. For comparative purposes, the pristine TiO_2, 3% IDT, and Aeroxide P-25 were also tested under similar experimental conditions.

4.3 Results and discussion

4.3.1 Characterisations of photocatalysts:

4.3.1.1 XRD:

Figure 4.1 (a) shows XRD plots of pristine TiO_2 and IDT nanoparticles. All diffraction peaks are associated with anatase phase corresponding to JCPDS card number 21-1272 of TiO_2, which shows that the crystalline structure of TiO_2 was preserved even after doping with iodine. Peaks of the TiO_2 corresponding to additional phases are not always perceived in patterns probably due to the highly dispersed TiO_2 or because XRD was not sensitive enough to detect such minor changes in TiO_2 [8]. The best phase of TiO_2 as a photocatalyst is anatase because it prolongs the life of e^-/h^+ pair with respect to other phases, which permits a charge carrier to take part in the reaction on the surface [9]. The synthesised photocatalysts' distinctive anatase peak (101) is depicted in Figure 4.1 (b). According to Figure 4.1 (b), the peak (101) changed to the lower 2θ value when the iodine concentration in TiO_2 increased, and doped catalyst peaks became broader than pristine TiO_2 peaks. [2]. The expansion of the XRD peaks towards lower 2θ value indicates decrease in the particle size according to Debye-Scherer formula [9]. Consequently, the specific surface area of the catalyst increases and the photocatalytic reaction rate increases [10].

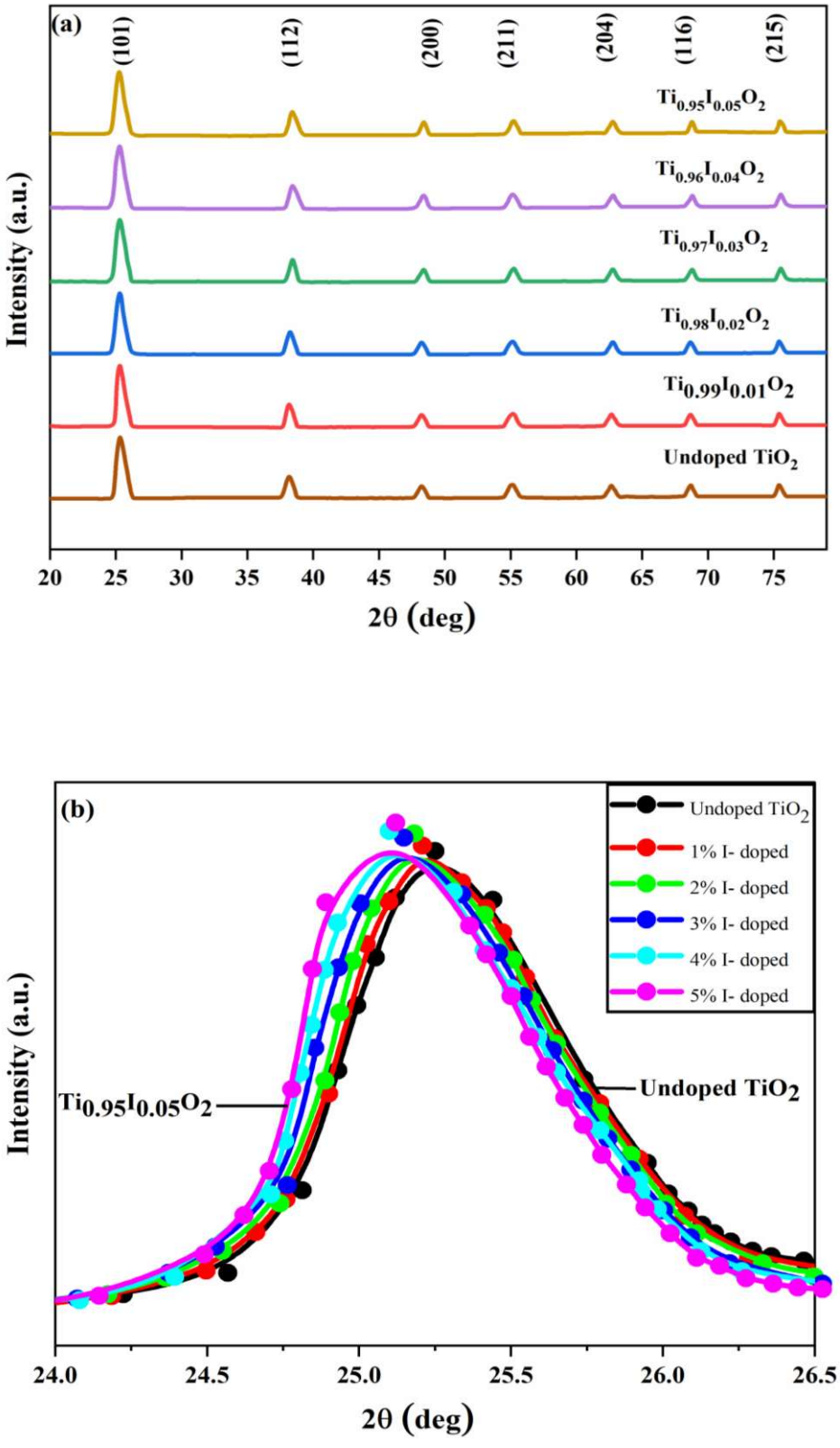

Figure 4.1 (a) XRD diagram of pristine and IDT nanoparticles (b) Characteristics synchrotron of TiO_2 at 2θ ranged from 24 to 26.5.

4.3.1.2 FTIR:

FTIR spectra was used to identify the functional groups in pristine TiO_2 and IDT nanoparticles.

Strong absorption was seen in all spectra between 500 and 1200 cm^{-1} because of the O–Ti–O bonding into the lattice vibrations of TiO_2. The band observed at 1620 cm^{-1} is ascribed to bending vibrations of the H-O-H bond for surface-adsorbed water molecules [1]. The hydroxyl stretching of surface adsorbed hydroxyl groups are shown at peaks at 3450 cm^{-1} [12]. Additionally, it can be seen that the incorporation of iodine doping enhances the strength of the absorption peaks associated with hydroxyl stretching and bending vibrations, and peaks also become more prominent as I-doping levels are increased [13]. Also, the broader peaks 1401 cm^{-1} are caused by H-I-H stretching and bending vibration caused by water or surface-absorbed hydroxyl groups [1,14].

Since the OH^- are the primary predator for the generated charge carrier that forms hydroxyl free radicals ($OH^{\cdot}$), required for dye degradation, confirm their improved photocatalytic activity [15]. After I doping in TiO_2, a sizable increase in OH group peak intensity was seen, indicating that iodine enriched the OH group in TiO_2 [16]. Ma et al. reveal that I doping in TiO_2 increased the OH groups [17]. The existence of a large number of OH groups in the synthesized photocatalysts ensures its better photocatalytic activity since the OH groups serve as the main scavenger for the photogenerated charge carrier that leads to the generation of hydroxyl radical ($OH^{\cdot}$) which is necessary for photodegradation of the dye. Steps of mechanism is given in section 4.3.2.1 [16].

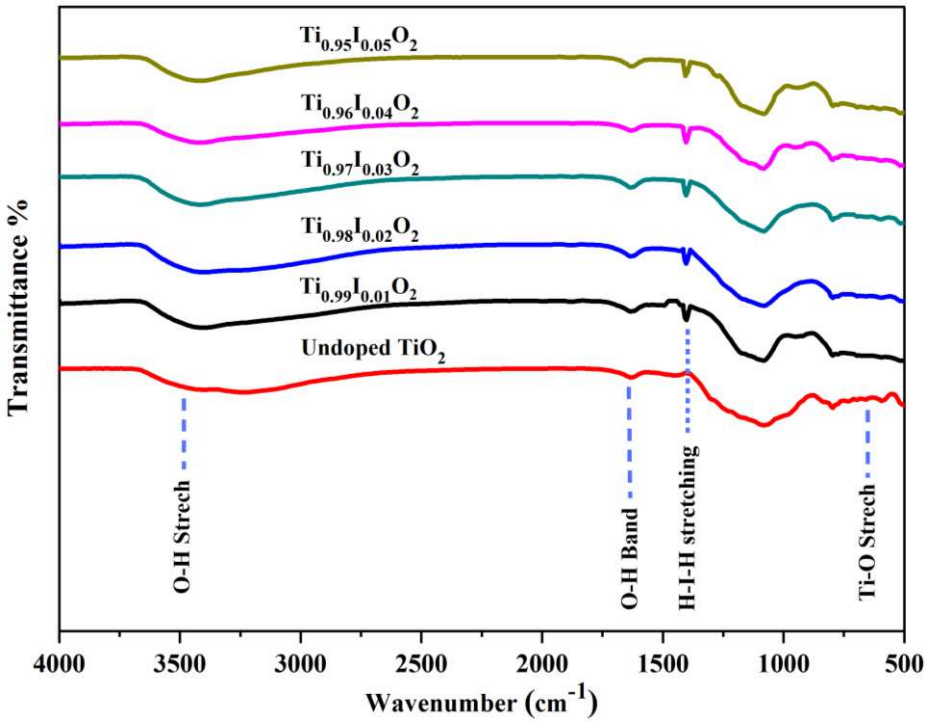

Figure 4.2 FTIR plots of pristine TiO_2 and IDT nanoparticles.

4.3.1.3 DRS:

The optical absorbance response of pristine TiO_2 and IDT photocatalysts is measured in the UV–visible spectrum shown in Figure 4.3.

The reduction in bandwidth brought on by the interconnection between I5p and Ti3d states, as well as the conversion of O2p to higher energy levels in Ti^{4+} in TiO_2, causes transfer of absorption band in TiO_2, doped with iodine [18]. TiO_2 band gap diminishes as Iodine concentration rises, and they are all smaller than the pristine TiO_2 band gap [17]. The reason for this is that I doping generates cracks in the TiO_2 crystal, resulting in defective energy levels and a rise in internal stress [20].

The values of band gap energy of pristine TiO_2 and 5% IDT are 3.2 and 1.95 eV respectively. The variation of band gap energy is depicted in the inset of Figure 4.3.

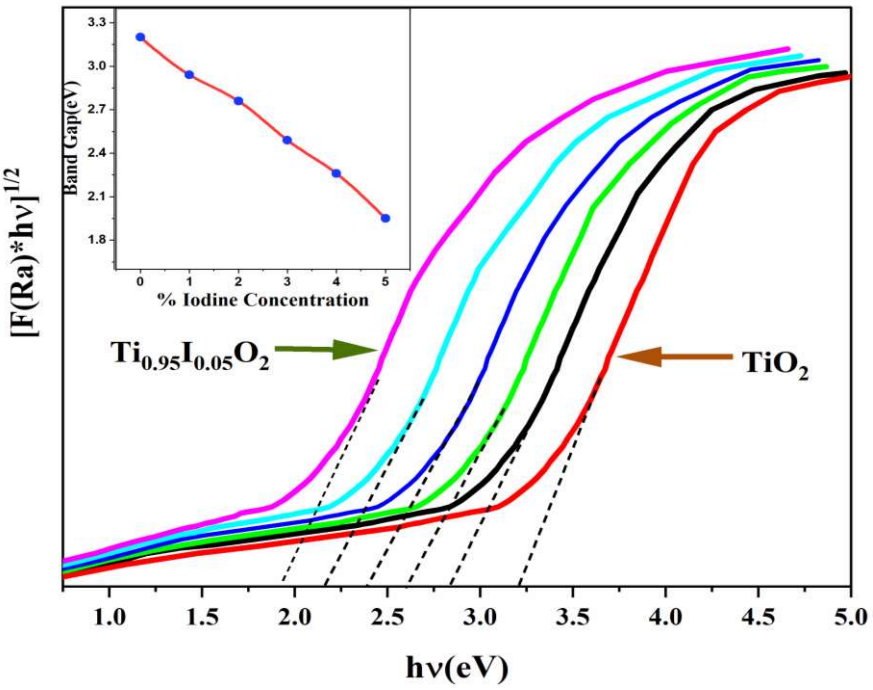

Figure 4.3 DRS plots of pristine and IDT (1-5%) nanoparticles.

4.3.1.4 XPS:

XPS analysis was performed on 3% IDT nanoparticles, and it approves the presence of Ti, O, and I elements and their oxidation states.

In Figure 4.4 (a), two peaks at 458.7 eV and 464.4 eV were assigned to $Ti2p_{3/2}$ and $Ti2p_{1/2}$ of TiO_2, respectively. These peaks are accredited to Ti^{3+} and Ti^{4+}, respectively. The peak at 458.7 eV is formed to maintain the electro-neutral nature because I^{5+} substitutes the Ti^{4+} into TiO_2 lattice. The existence of these peaks of titania enhances the photocatalytic activity due to surface-adsorbed oxygen [21]. Ti^{3+} is associated with oxygen vacancies and surface defects, which act as electron traps to extend charge separation and reduce recombination rates, thereby boosting the efficiency of photocatalytic reactions. Ti^{4+}, the dominant titanium state, forms stable Ti-O bonds in the lattice, maintaining structural integrity [22].

Figure 4.4 (b) shows two peaks of oxygen; the peak at 530.1 eV corresponds to lattice oxygen, and the peak at 531.7 eV represents chemisorbed oxygen peak (OH^-) [23]. The presence of surface-adsorbed oxygen facilitates the direct combination with photogenerated electrons, generating anion radicals. These anion radicals play a crucial role in the degradation of MB dye [24]. The OH^- ions exhibit high reactivity and instability. They can react with the holes on TiO_2 surface, leading to the formation of $OH^·$ radicals. These radicals play a significant role in the degradation of dye molecules [16]. Zhao et al. also confirmed that hydroxyl ions enhance photocatalytic degradation [25].

In Figure 4.4 (c), two doublet peaks at 624.02 (I $3d_{5/2}$) and 635.77 eV (I $3d_{3/2}$) and at 620 (I $3d_{3/2}$) and 632.08 (I $3d_{5/2}$) eV are shown. Tojo et al. reported peaks at 624.02 and 620 eV are attributed to I^{5+} and I^-, respectively [26]. There is a difference between binding energy of I $3d_{3/2}$ of the synthesised photocatalyst and HIO_3 (622 eV) due to the energetically favourable replacement of Ti^{4+} with I^{5+}. This happens because the ionic radius of Ti^{4+} (0.064 nm) and I^{5+} (0.062 nm) are very close. I^{5+} exist in the form of Ti–O–I bond in TiO_2, and I^- is derived from I^{5+} reduction by accepting electrons [27]. This formation of Ti-O-I bonds, narrows the bandgap, allowing the material to absorb more visible light and enhancing its photocatalytic activity, particularly in dye degradation. The Ti-O-I bonding also aids in the efficient generation of reactive oxygen species (ROS) and hydroxyl radicals, crucial for breaking down pollutants under light irradiation. This series of modifications significantly advances the photocatalytic capabilities of TiO_2 under practical conditions [28].

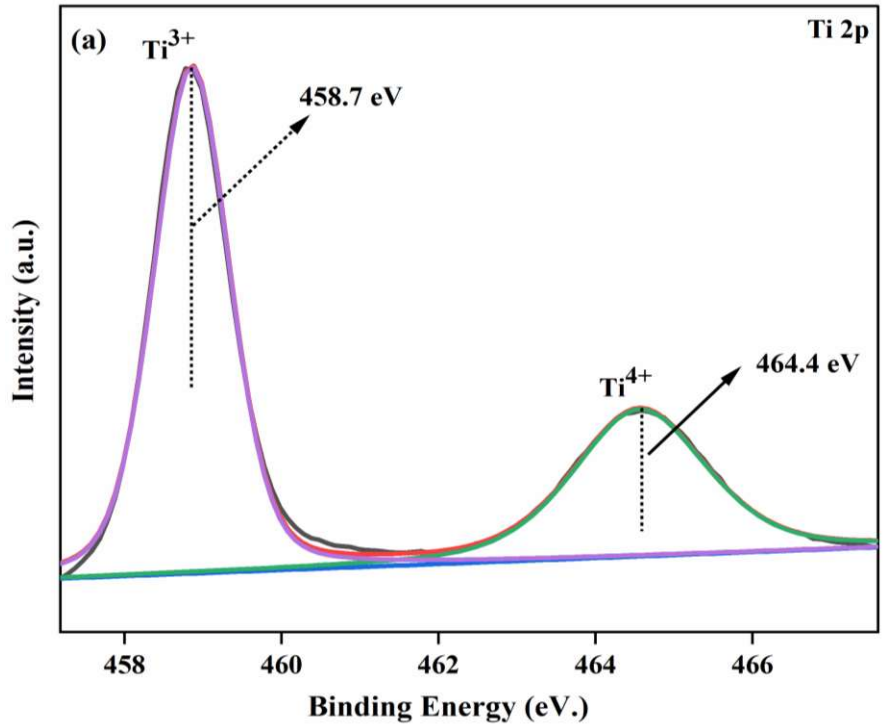
(a)
Ti 2p
Ti3+
458.7 eV
Ti4+
464.4 eV
Intensity (a.u.)
458
460
462
464
466
Binding Energy (eV.)

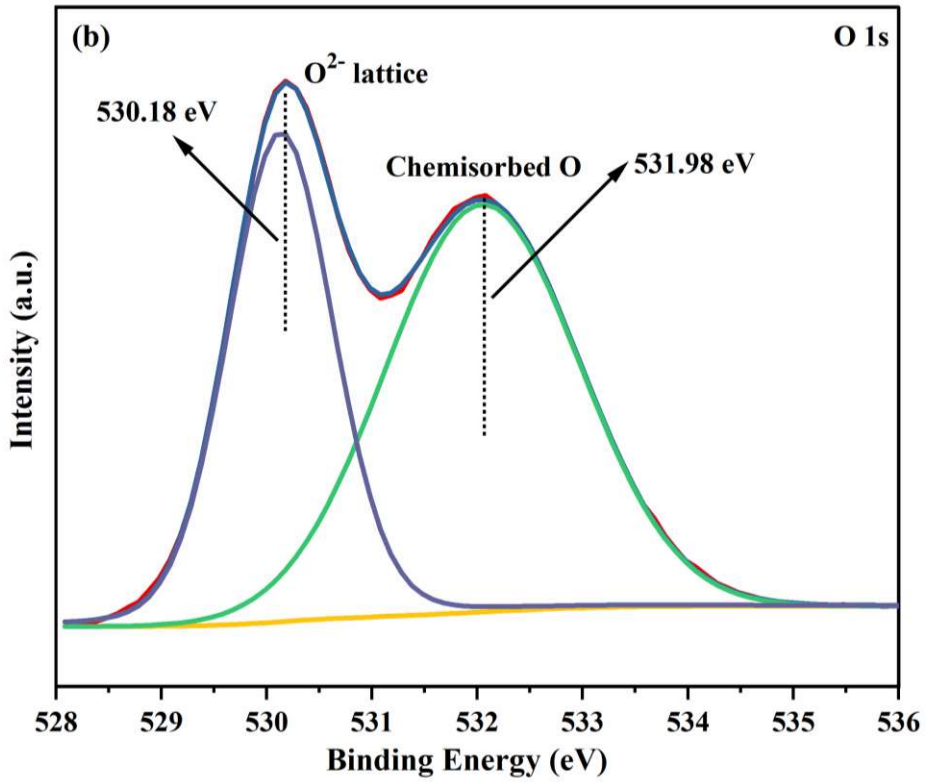
(b)
O 1s
O2- lattice
530.18 eV
Chemisorbed O
531.98 eV
Intensity (a.u.)
528
529
530
531
532
533
534
535
536
Binding Energy (eV)

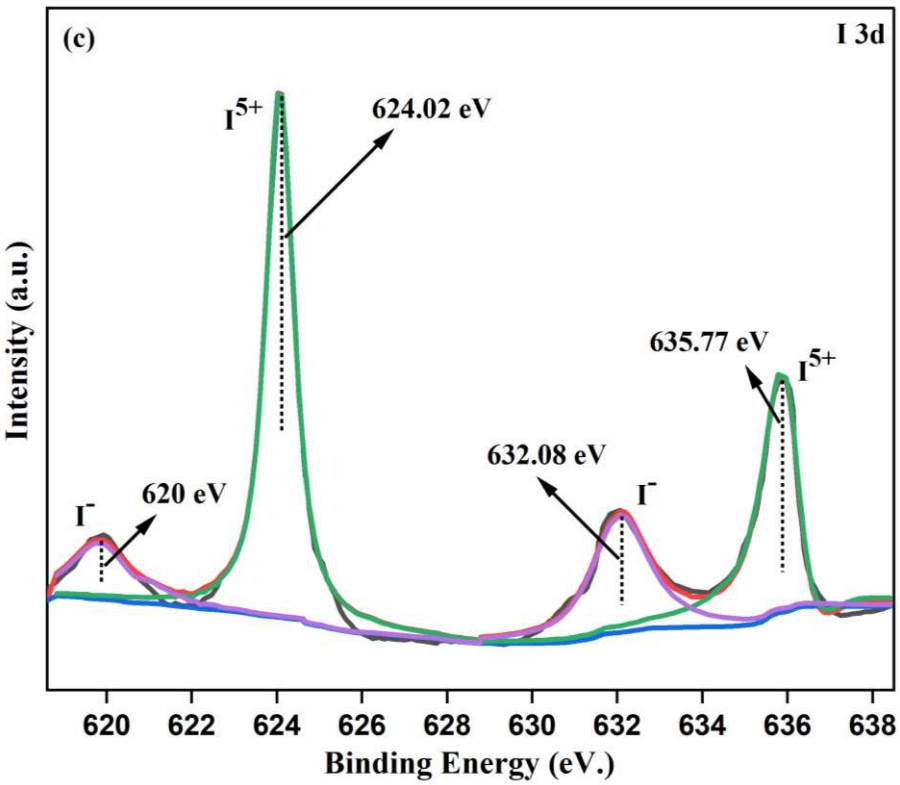

Figure 4.4 XPS patterns of (a) Ti 2p, (b) O 1s, (c) I 3d spectrum for 3% IDT

4.3.2 Photocatalytic degradation of pristine and IDT nanoparticles:

4.3.2.1 Mechanism

The reaction mechanism of TiO_2 nanoparticles doped with iodine was assessed in terms of dye degradation. The following equations represent the dye degradation mechanism and significance of iodine in photocatalysis [3,4,6,16,29,30].

$$TiO_2 + h\nu \rightarrow TiO_2\,(h^+ + e^-) \quad (4.1)$$

$$h^+ + e^- \rightarrow Heat \quad (4.2)$$

$$e^- + O_{2(ads)} \rightarrow O_2^{-}\cdot \quad (4.3)$$

$$O_2^{-}\cdot + h^+ \rightarrow O^{-}\cdot \quad (4.4)$$

$$O^{-}\cdot + H_2O_{(ads)} \rightarrow OH\cdot + OH^- \quad (4.5)$$

$$h^+ + H_2O_{(ads)} \rightarrow OH^- + H^+ \quad (4.6)$$

$$OH^- + h^+ \rightarrow OH\cdot \quad (4.7)$$

$$H^+ + O^{-\cdot} \rightarrow OH\cdot \quad (4.8)$$

$$IO_3^- + heat \rightarrow HIO_3 \quad (4.9)$$

$$2HIO_3 + heat \rightarrow I_2O_5 + H_2O \quad (4.10)$$

$$I_2O_5 + H_2O + O_2 \rightarrow 2HIO_4 \quad (4.11)$$

$$HIO_4 \rightarrow IO_4^- + H^+ \quad (4.12)$$

$$IO_4^- + UV\ light \rightarrow IO_3^{\cdot} + O^{\cdot -} \quad (4.13)$$

$$OH\cdot + IO_4^- \rightarrow OH^- + IO_4^{\cdot} \quad (4.14)$$

$$O^{-\cdot} + MB \rightarrow simple\ product \quad (4.15)$$

$$OH\cdot + MB \rightarrow simple\ product \quad (4.16)$$

$$IO_4^{\cdot} + MB \rightarrow simple\ product \quad (4.17)$$

It is clear from equations that when iodine is doped in TiO_2, various species, such as IO_4^- /IO_3^-/I^- are formed and have played an essential part in improving the photocatalytic performance of catalysts in degradation of MB dye. Chao-Yin Kuo et al. [6] found the photocatalytic mechanism of IO_4^- under UV light to degrade dye. High activity is caused by the creation of numerous highly reactive species ($IO_4^{\cdot}$ and $IO_3^{\cdot}$), and non-reactive intermediates (IO_4^- and IO_3^-) are also cited by Chien-Hwa Yu et al. [31]. It is also confirmed from XPS analysis that additional states of Iodine (I^{5+}) shows improved charge carrier separation, which prevents charge carrier recombination since I^{5+} serves as an electron acceptor [32]. The generated holes (Eq. 4.1) can directly combine with surface adsorbed hydroxyl groups (OH^-) to form $OH^{\cdot}$ radicals (Eq. 4.7) which are crucial for photodegradation of the dye. Therefore, above reactions indicate that the formation of highly reactive radicals ($O_2^{-\cdot}$, $OH^{\cdot}$, $IO_3^{\cdot}$ and $IO_4^{\cdot}$) and non-radical intermediates (IO_4^- and IO_3^- responsible for the degradation of the dye [2].

4.3.2.2 Kinetic Study:

The adsorption investigation revealed that only a small fraction, approximately 1-2%, of the dye was adsorbed on the nanoparticles' surface. It is also essential for photodegradation of the dye. In the absence of photocatalysts in UV light, minimal photodegradation of the dye occurred. The dye did not show any tendency of self-degradation as determined with the procedure discussed earlier.

All the catalysts' kinetic analysis was completed, and Figure 4.5 and Figure 4.6 depicts kinetic data for degradation of MB dye in its aqueous solution with 3% IDT. The data were analysed by pseudo first order kinetics given by 4.18 and solving it gives -ln (C/Co) = $-k_pC$, where k_p is rate constant (apparent), C is concentration at time t and Co is the initial concentration.

$$-dC/dt = k_pC \tag{4.18}$$

The reaction rate constant for degradation of MB dye of the undoped and IDT are given in Table 4.2 along with R^2 values. These results are similar to those obtained when Orange II dye was photodegraded using a doped TiO_2 photocatalyst, where data of the photodegradation process were obtained employing a pseudo-first-order rate equation [33]. The results of photodegradation show that the photocatalytic activity of synthesised nanoparticles surges with surging the iodine concentration up to 3%, but the activity of nanoparticles decreases at higher concentrations of iodine (4-5% IDT) because the higher concentration of iodine creates charge recombination centres or shields [5].

Table 4.2 Summary of the degree of fitting (R^2) and reaction rate constants of the undoped and IDT photocatalysts.

	10 ppm		**20 ppm**		**30 ppm**		**40 ppm**		**50 ppm**	
Catalyst	k_p	R^2	k_p	R^2	k_p	R^2	k_p	R^2	k_p	R^2
Undoped	0.035	0.988	0.035	0.974	0.034	0.992	0.033	0.981	0.032	0.972
1% IDT	0.038	0.992	0.037	0.980	0.036	0.965	0.034	0.965	0.033	0.983
2% IDT	0.041	0.986	0.040	0.965	0.039	0.992	0.039	0.998	0.038	0.995
3% IDT	0.049	0.996	0.048	0.986	0.047	0.982	0.047	0.995	0.046	0.963
4% IDT	0.045	0.984	0.044	0.996	0.044	0.956	0.044	0.975	0.043	0.964
5% IDT	0.041	0.996	0.040	0.964	0.040	0.974	0.039	0.984	0.039	0.998

k_p is in min^{-1}

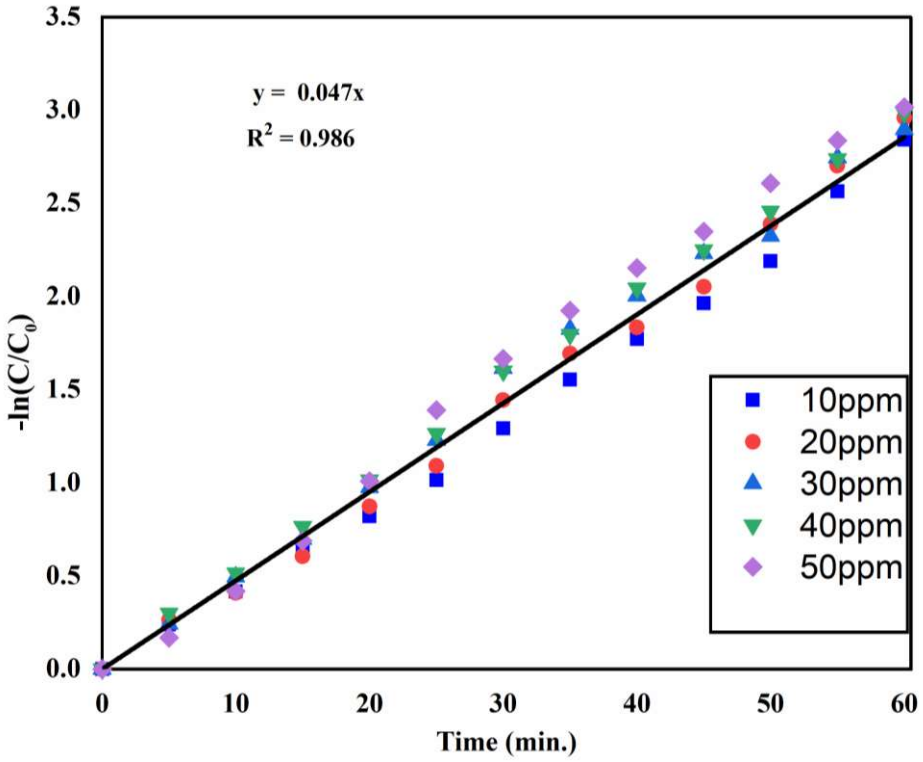

Figure 4.5 Kinetic study of MB dye degradation for 3% IDT nanoparticles

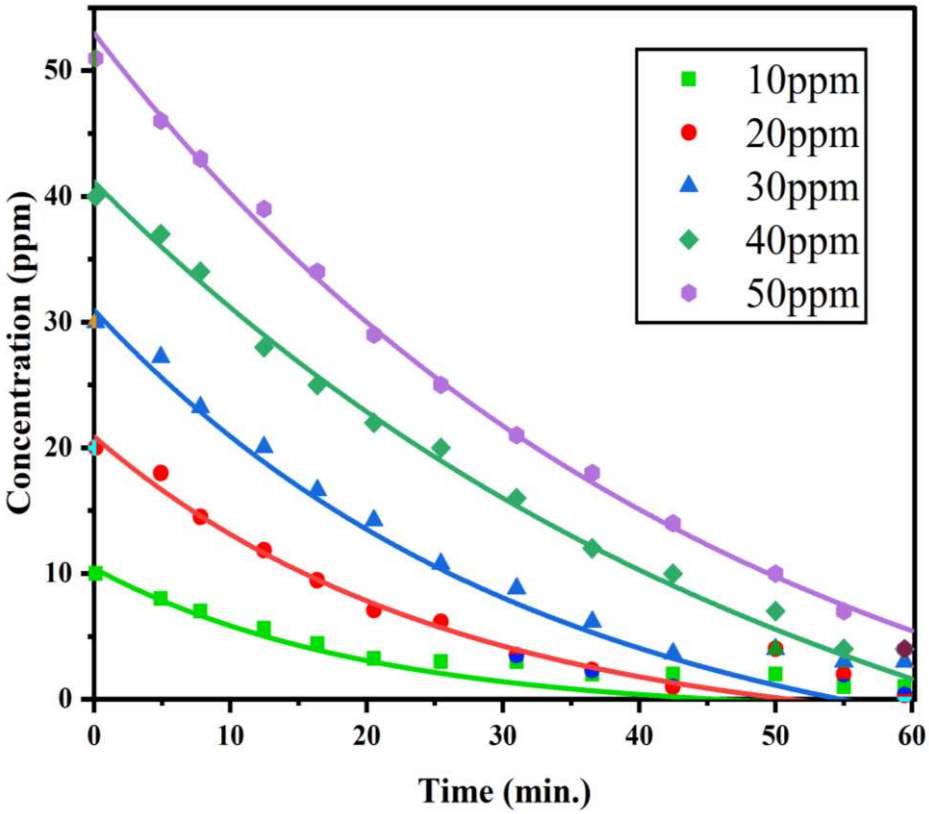

Figure 4.6 Variation of initial concentration of MB during degradation with time with 3% IDT photocatalyst

4.3.3 Photocatalytic degradation study of MB dye with pristine TiO_2 and IDT photocatalysts

Several experiments were conducted to assess the photocatalytic activity of 3% IDT and pristine TiO_2 photocatalysts at different reaction parameters in UV light. Two sets of tests were conducted for MB dye degradation without any catalyst, one with UV light and one without, for 1 h. The results indicate that MB dye degradation was not affected by UV light. A 100 mL dye solution with 0.01 g of catalyst was stirred in a quartz tube for 1 h in dark. The absorbance of dye solution was slightly shifted after treatment due to the adsorption-desorption equilibrium between the catalyst and MB solution, with UV light not turned on. The stirring was on for an hour under UV illumination in a quartz tube.

The decreased absorbance of the dye solution indicated that UV light activated the catalyst and produced hydroxyl ions that degraded dye molecules. Therefore, it can be concluded that there is a mutual dependence on catalysts and light [34].

The study examined how photocatalysts perform under different pH conditions, initial dye concentration, and catalyst amount to find the optimum parameters. While investigating these parameters, one was changed while others remained constant. Various parameters like pH, catalyst loading and initial concentration of dye affect the process of degradation of MB. The effect of these parameters has been studied and given below:

4.3.3.1 Effect of initial pH:

The pH significantly influences the photocatalytic degradation reaction for the MB dye solution. To investigate the degradation process under UV radiation, pristine and IDT catalysts were used, and the initial pH was varied from 4 to 9, as shown in Figure 4.7. There is no significant difference in acidic as well as basic conditions in degradation rate of MB under UV light. Interestingly, degradation rate of MB was higher at neutral pH compared to other pH [35]. The explanation is that under acidic conditions, TiO_2 photocatalysts tend to agglomerate, reducing the available surface area for dye adsorption and photon absorption. This aggregation results in a lower dye removal efficiency. At higher pH values, OH^- ions react with photogenerated h^+ to form $OH\cdot$ radicals. These radicals are quickly scavenged without reacting with the dyes, leading to a reduction in dye removal efficiency [2].

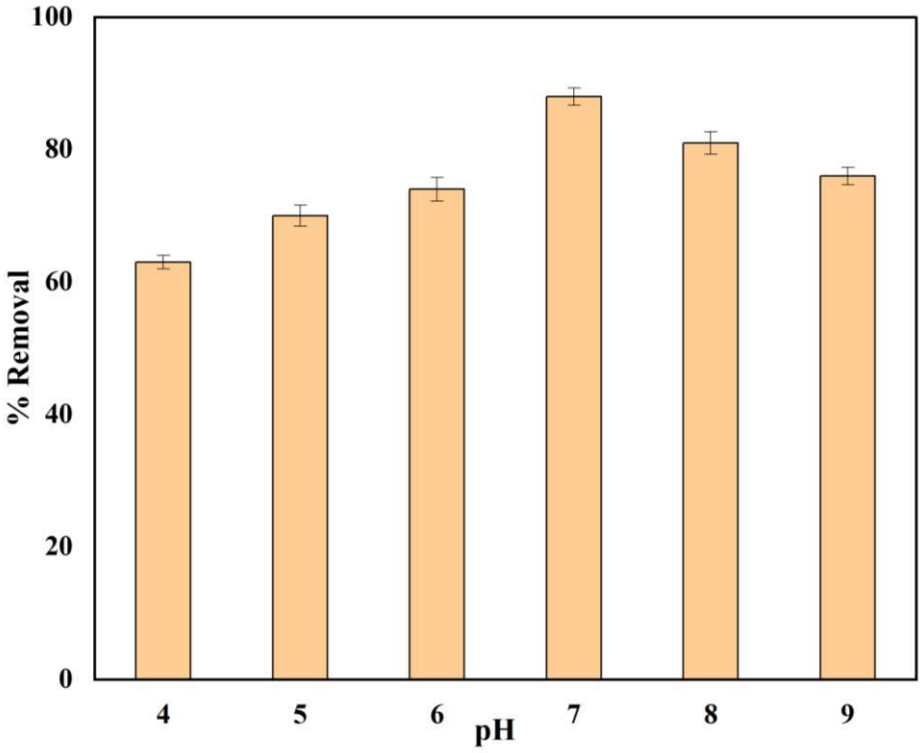

Figure 4.7 Effect of pH on removal of MB dye (30 ppm) by 3% IDT photocatalyst at catalyst dose of 0.1 g L^{-1}

4.3.3.2 Effect of catalyst loading:

The influence of catalyst loading on MB dye degradation was examined by varying the amount of TiO_2 catalyst within the range of 0.025 to 0.150 g L^{-1}. The initial dye concentration remained constant throughout the experiments at 30 ppm, and the pH was maintained at 7 and experiment was done for 40 min. The results indicate that the optimal catalyst loading for degradation of MB dye is 0.1 g L^{-1}, which exhibited the highest degradation rate. When the catalyst loading is below 0.1 g L^{-1}, few catalyst particles are available relative to the dye particles. As a result, the degradation process is slowed down due to lower availability of catalyst sites.

Conversely, increasing catalyst dosage beyond 0.1 g L^{-1} does not significantly improve the degradation rate. This is because of the increased turbidity of the solution as the

catalyst dosage increases. The higher turbidity obstructs penetration of UV light, thereby impeding the activation of catalyst particles and reducing the overall degradation rate. Therefore, 0.1 g L^{-1} is the optimal catalyst loading, as evidenced by Figure 4.8. which maintains a balance between providing sufficient catalyst particles for effective dye degradation and maintaining a clear solution that allows efficient UV light penetration [34].

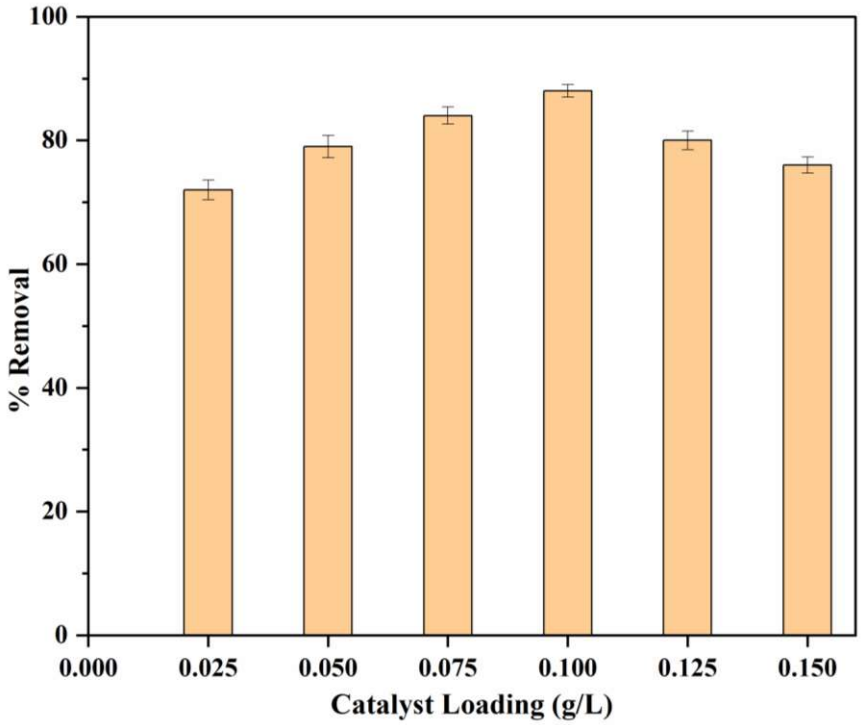

Figure 4.8 Effect of catalyst loading on the removal of MB dye (30 ppm) by 3% IDT photocatalyst at 7 pH

4.3.3.3 Effect of initial dye concentration:

The present study investigated the impact of varying initial dye concentrations, ranging from 10 to 50 ppm, on photocatalytic degradation, as shown in Figure 4.9. The experiments were conducted at pH 7 and a catalyst loading of 0.1 g L^{-1} for 1 h in UV light. The findings revealed a decline in the degradation efficiency as initial MB dye

concentration varied from 10 to 50 ppm. At lower concentrations, the degradation occurred through the action of hydroxyl/superoxide radicals formed during the catalyst excitation by UV light. However, the light penetration within the dye solution became more challenging at high concentrations. This reduced the absorption of light at catalyst surface, directly impacting the degradation efficiency by reducing the formation of superoxides [36].

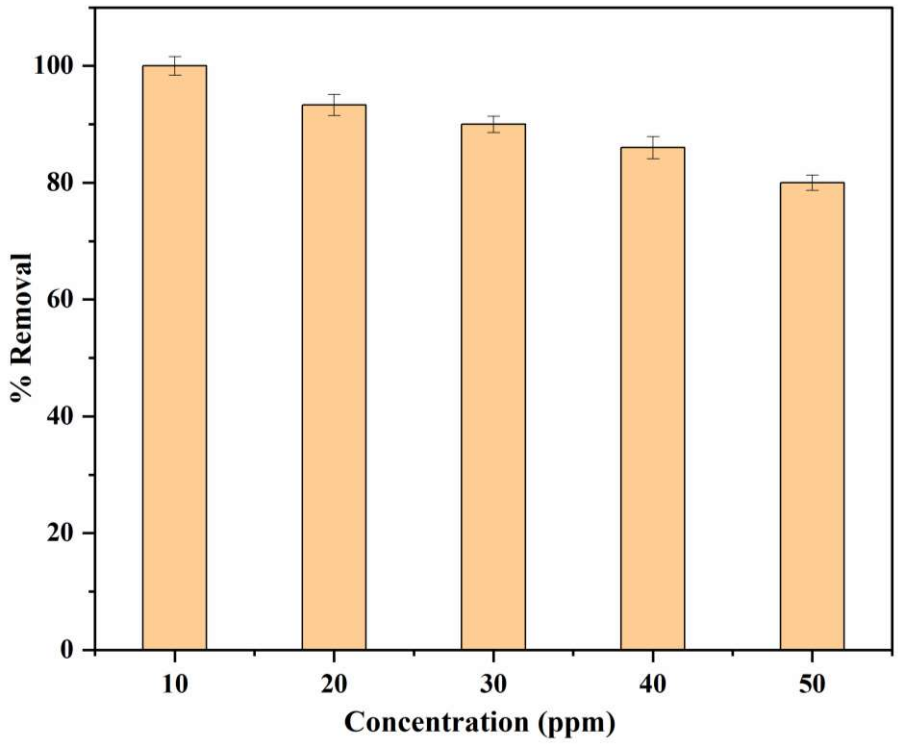

Figure 4.9 Effect of initial dye concentration on the removal of MB dye by 3% IDT photocatalyst at catalyst dose of 0.1 g L^{-1} and 7 pH.

4.3.4 Regeneration of the catalyst:

It is crucial that photocatalysts can be reused for economic viability. The best IDT photocatalyst (3% I-doped) was regenerated after use as per procedure discussed in section 2.3.5. and use repeatedly for degradation of MB dye. Figure 4.10. depicts the

results of our best photocatalyst's repeatability experiments, i.e. The tests were done 5 times in a row so that the ability of the catalyst to degrade MB could be studied. The initial MB concentration was 30 mg L^{-1} at 7 pH and an irradiation time of 1 h. As stated, the degradation efficiency went from 88% for the first cycle to 77.87% for the fifth cycle. So, after five repeatability tests, there is only 10.13% drop in the degradation rate. Figure 4.10. also shows that the shapes of all the curves are almost the same. The drop may be because of the agglomeration of the catalyst several times during heat treatment [37]. Huang et al. [38] also said that the TiO_2 photocatalyst has the possibility of agglomeration of catalyst during heat treatment and causing loss of the catalytic performance.

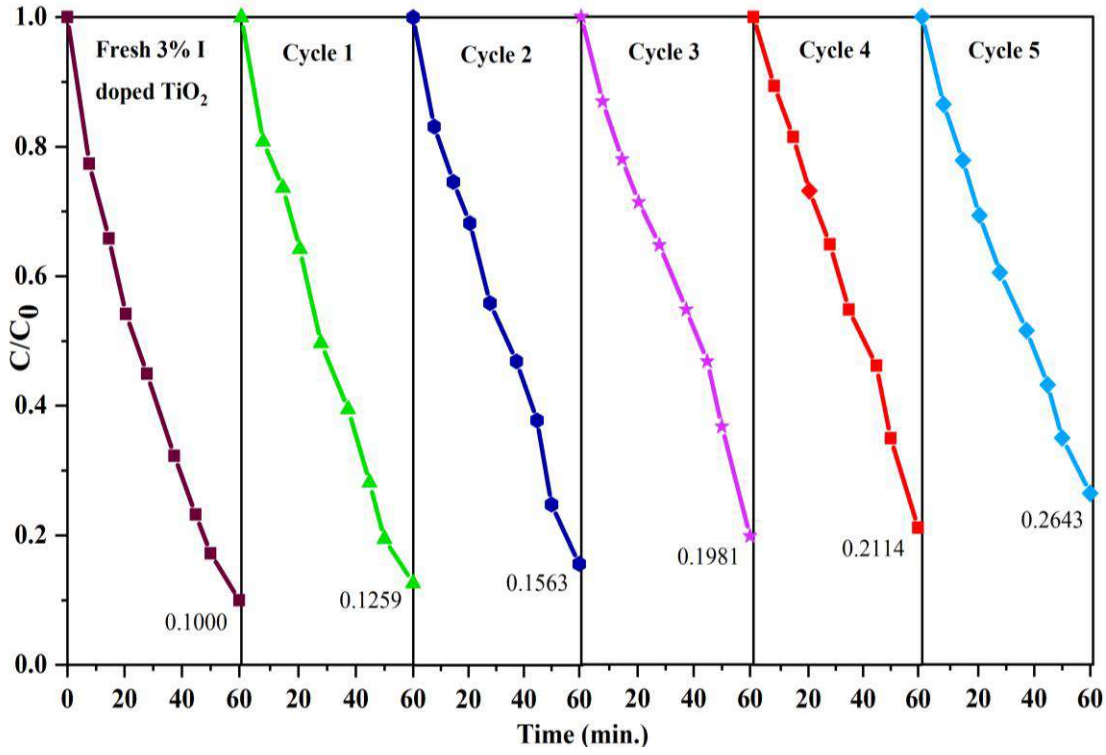

Figure 4.10 Performance of regenerated 3% IDT photocatalyst for degradation of MB dye (30 ppm) at catalyst dose of 0.1 g L^{-1} and 7 pH.

4.3.5 Comparison among the best doped photocatalyst ($Ti_{0.97}I_{0.03}O_2$), undoped TiO_2, and Aeroxide P-25

Undoped TiO_2 and 3% IDT photocatalysts were compared to commercially available Aeroxide P-25 for photocatalytic activity. The findings are displayed in Figure 4.11. The 3% IDT photocatalyst exhibits the maximum photocatalytic degradation among all of these photocatalysts, as depicted in Figure 4.11.

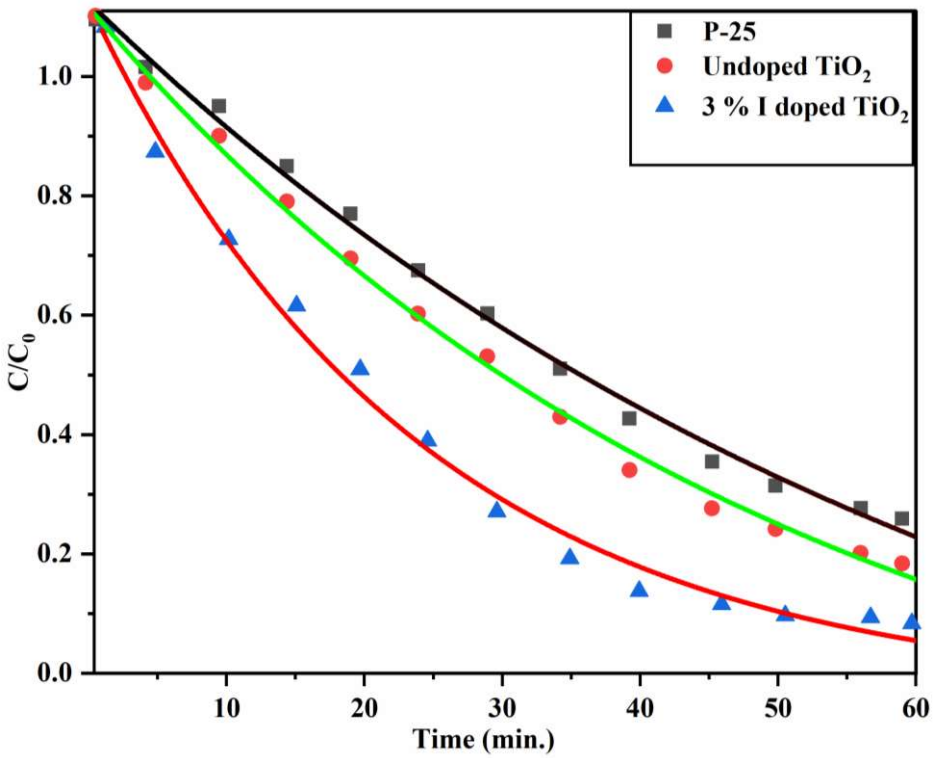

Figure 4.11 Comparison of the undoped TiO_2, 3% IDT, and Aeroxide P-25 for degradation of MB dye (30 ppm) at catalyst dose of 0.1 g L^{-1} and 7 pH.

4.3.6 Phytotoxicity

A phytotoxicity study was conducted to examine the toxic effects of MB dye on mung bean seeds. The findings are presented in Table 4.3 and Figure 4.12. The MB dye was harmful to plants, negatively impacting seed germination and seedling growth and inhibiting overall plant development [39]. When mung bean seeds were treated with MB

solution, their root and shoot lengths were shorter than those treated with distilled water and degraded MB solution. The toxicity of the MB dye was substantially diminished when it was subjected to photocatalytic degradation. After 7 days of incubation, the root and shoot lengths of mung beans treated with the degraded dye were significantly greater than those of untreated mung beans exposed to MB. These results suggest that its harmful effects can be reduced substantially by degrading the MB dye.

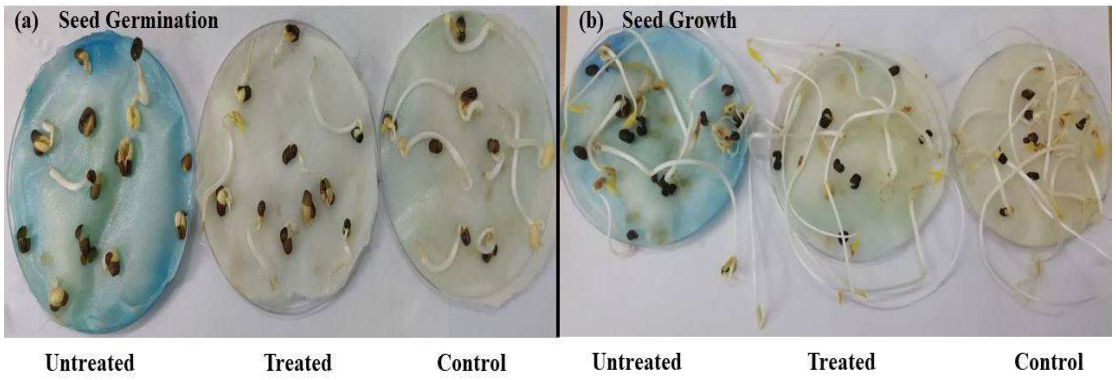

Figure 4.12 (a) Seed germination of control, Treated and untreated sample at t = 2 days (b) Seed growth of control, Treated and untreated sample at t = 7 days

Table 4.3 Toxicity assessment of residual MB solution after photodegradation on Vigna radiata seeds in control, treated and untreated samples.

Sample	Root Length (cm)	Shoot Length (cm)	% RG	% SG	PIN	% GIN
Treated	4.1	17	93.18	90	6.82	83.86
Untreated	2.6	14.5	59.09	70	40.91	41.36
Control	4.4	22	100	90	0	90

4.4 Conclusion:

The solution-combustion procedure was successfully employed to prepare pristine and IDT photocatalysts with iodine concentrations ranging from 0.00 to 0.05. The photocatalytic activity of each prepared photocatalyst was assessed using a UV-PCR reactor by UV light. The kinetic analysis shows that photocatalytic activity of the 3% IDT nanoparticles was the highest among all the synthesised photocatalysts. Interestingly, the study found that photocatalytic activity of TiO_2 increased as the iodine concentration reached 3%. However, beyond this doping concentration, the photocatalytic activity started to decrease. This suggests that 3% iodine doping is optimised for the photocatalytic performance of TiO_2. Furthermore, a comparative analysis was conducted between the synthesised pristine TiO_2, 3% IDT, and Aeroxide P-25 photocatalysts, demonstrating that the 3% IDT photocatalyst exhibited superior performance compared to the pristine TiO_2 and Aeroxide P-25 photocatalysts. In addition to assessing the potential use of treated water, a phytotoxicity study was also done. The results indicated that the treated water may be suitable for irrigation, suggesting that the photocatalytic degradation process effectively reduced the toxicity of pollutants in the water.

References

[1] R.P. Barkul, M.K. Patil, S.M. Patil, V.B. Shevale, S.D. Delekar, Sunlight-assisted photocatalytic degradation of textile effluent and Rhodamine B by using iodine doped TiO_2 nanoparticles, J. Photochem. Photobiol. A Chem. 349 (2017) 138–147. https://doi.org/10.1016/j.jphotochem.2017.09.011

[2] S. Saroj, L. Singh, S.V. Singh, Solution-combustion synthesis of anion (iodine) doped TiO_2 nanoparticles for photocatalytic degradation of Direct Blue 199 dye and regeneration of used photocatalyst, J. Photochem. Photobiol. A Chem. 396 (2020) 112532. https://doi.org/10.1016/j.jphotochem.2020.112532

[3] S. Bagwasi, B. Tian, F. Chen, J. Zhang, Synthesis, characterization and application of iodine modified titanium dioxide in phototcatalytical reactions under visible light irradiation, Appl. Surf. Sci. 258 (2012) 3927–3935. https://doi.org/10.1016/j.apsusc.2011.12.066

[4] W. Su, Y. Zhang, Z. Li, L. Wu, X. Wang, J. Li, X. Fu, Multivalency iodine doped TiO2: Preparation, characterization, theoretical studies, and visible-light

photocatalysis, Langmuir 24 (2008) 3422–3428. https://doi.org/10.1021/la701645y

[5] Q. Zhang, Y. Li, E.A. Ackerman, M. Gajdardziska-Josifovska, H. Li, Visible light responsive iodine-doped TiO_2 for photocatalytic reduction of CO_2 to fuels, Appl. Catal. A Gen. 400 (2011) 195–202. https://doi.org/10.1016/j.apcata.2011.04.032

[6] C.Y. Kuo, H.M. Hsiao, Preparation of iodine doped titanium dioxide to photodegrade aqueous bisphenol A under visible light, Process Saf. Environ. Prot. 95 (2015) 265–270. https://doi.org/10.1016/j.psep.2015.03.013

[7] M.A. Budihardjo, B.S. Ramadan, R.P. Safitri, A.J. Effendi, S. Hidayat, Y.V. Paramitadevi, B. Ratnawati, Metals Removal from Contaminated Soil Using Electrokinetic Treatment – Effect of Different Permeable Reactive Barrier and Flushing Solution, Ecol. Eng. Environ. Technol. 24 (2023) 19–27. https://doi.org/10.12912/27197050/156969.

[8] R.P. Cavalcante, R.F. Dantas, B. Bayarri, O. González, J. Giménez, S. Esplugas, A. Machulek, Synthesis and characterization of B-doped TiO_2 and their performance for the degradation of metoprolol, Catal. Today 252 (2015) 27–34. https://doi.org/10.1016/j.cattod.2014.09.030

[9] S. Mustapha, J.O. Tijani, M.M. Ndamitso, A.S. Abdulkareem, D.T. Shuaib, A.T. Amigun, H.L. Abubakar, Facile synthesis and characterization of TiO2 nanoparticles: X-ray peak profile analysis using Williamson–Hall and Debye–Scherrer methods, Int. Nano Lett. 11 (2021) 241–261. https://doi.org/10.1007/s40089-021-00338-w.

[10] F. Azeez, E. Al-Hetlani, M. Arafa, Y. Abdelmonem, A.A. Nazeer, M.O. Amin, M. Madkour, The effect of surface charge on photocatalytic degradation of methylene blue dye using chargeable titania nanoparticles, Sci. Rep. 8 (2018) 1–9. https://doi.org/10.1038/s41598-018-25673-5.

[11] T. Luttrell, S. Halpegamage, J. Tao, A. Kramer, E. Sutter, M. Batzill, Why is anatase a better photocatalyst than rutile? - Model studies on epitaxial TiO_2 films, Sci. Rep. 4 (2015) 1–8. https://doi.org/10.1038/srep04043

[12] J. Matos, S. Miralles-Cuevas, A. Ruíz-Delgado, I. Oller, S. Malato, Development of TiO_2-C photocatalysts for solar treatment of polluted water, Carbon N. Y. 122 (2017) 361–373. https://doi.org/10.1016/j.carbon.2017.06.091

[13] X. Chen, H. Sun, J. Zhang, O. Ahmed Zelekew, D. Lu, D.H. Kuo, J. Lin, Synthesis of visible light responsive iodine-doped mesoporous TiO_2 by using biological renewable lignin as template for degradation of toxic organic pollutants, Appl. Catal. B Environ. 252 (2019) 152–163. https://doi.org/10.1016/j.apcatb.2019.04.034

[14] Y. Wang, J. Ren, G. Liu, P. Peng, Synthesis and characterization of iodine ion doped mesoporous TiO_2 by sol-gel method, Mater. Chem. Phys. 130 (2011) 493–499. https://doi.org/10.1016/j.matchemphys.2011.07.020

[15] T. Ali, P. Tripathi, A. Azam, W. Raza, A.S. Ahmed, A. Ahmed, M. Muneer, Photocatalytic performance of Fe-doped TiO_2 nanoparticles under visible-light irradiation, Mater. Res. Express 4 (2017). https://doi.org/10.1088/2053-1591/aa576d

[16] S. Saroj, L. Singh, S.V. Singh, Solution-combustion synthesis of anion (iodine) doped TiO_2 nanoparticles for photocatalytic degradation of Direct Blue 199 dye and regeneration of used photocatalyst, J. Photochem. Photobiol. A Chem. 396 (2020) 112532. https://doi.org/10.1016/j.jphotochem.2020.112532

[17] Y. Ma, J.W. Fu, X. Tao, X. Li, J.F. Chen, Low temperature synthesis of iodine-doped TiO_2 nanocrystallites with enhanced visible-induced photocatalytic activity, Appl. Surf. Sci. 257 (2011) 5046–5051. https://doi.org/10.1016/j.apsusc.2011.01.019

[18] R. Long, Y. Dai, B. Huang, Structural and electronic properties of iodine-doped anatase and rutile TiO_2, Comput. Mater. Sci. 45 (2009) 223–228. https://doi.org/10.1016/j.commatsci.2008.09.011

[19] C. Red, Z.-K. Tio, Z. Liu, W. Zhang, X. Zhao, X. Sheng, Z. Hu, Q. Wang, Z. Chen, S. Wang, X. Zhang, X. Wang, Efficient Adsorption-Assisted Photocatalysis Degradation of, (2022) 1–15

[20] M. Long, W. Cai, Z. Wang, G. Liu, Correlation of electronic structures and crystal structures with photocatalytic properties of undoped, N-doped and I-doped TiO_2, Chem. Phys. Lett. 420 (2006) 71–76. https://doi.org/10.1016/j.cplett.2005.12.036

[21] Q. Sun, C. Yang, J. Li, W. Aboshora, H. Raza, L. Zhang, Highly efficient trans-cis isomerization of lycopene catalyzed by iodine-doped TiO_2 nanoparticles, RSC Adv. 6 (2016) 1885–1893. https://doi.org/10.1039/c5ra24074c

[22] W. Li, R. Liang, A. Hu, Z. Huang, Y.N. Zhou, Generation of oxygen vacancies in visible light activated one-dimensional iodine TiO_2 photocatalysts, RSC Adv. 4 (2014) 36959–36966. https://doi.org/10.1039/c4ra04768k.

[23] S. Saroj, L. Singh, R. Ranjan, S.V. Singh, Enhancement of photocatalytic activity and regeneration of Fe-doped TiO_2 ($Ti_{1-x}Fe_xO_2$) nanocrystalline particles synthesized using inexpensive TiO_2 precursor, Res. Chem. Intermed. 45 (2019) 1883–1906. https://doi.org/10.1007/s11164-018-3708-2

[24] X. Wang, J. Song, J. Huang, J. Zhang, X. Wang, R.R. Ma, J. Wang, J. Zhao, Activated carbon-based magnetic TiO_2 photocatalyst co-doped with iodine and nitrogen for organic pollution degradation, Appl. Surf. Sci. 390 (2016) 190–201. https://doi.org/10.1016/j.apsusc.2016.08.040

[25] Y. Zhao, L. Zhu, Y. Yu, F. Gao, W. Wang, D. Chen, X. Zhao, Facile one-pot preparation of Ti^{3+}, N co-doping TiO_2 nanotube arrays and enhanced photodegradation activities by tuning tube lengths and diameters, Catal. Today 355 (2020) 563–572. https://doi.org/10.1016/j.cattod.2019.06.051

[26] S. Tojo, T. Tachikawa, M. Fujitsuka, T. Majima, Iodine-doped TiO_2 photocatalysts: Correlation between band structure and mechanism, J. Phys. Chem. C 112 (2008) 14948–14954. https://doi.org/10.1021/jp804985f

[27] Z. He, Y. Yu, D. Wang, J. Tang, J. Chen, S. Song, Photocatalytic reduction of carbon dioxide using iodine-doped titanium dioxide with high exposed {001} facets under visible light, RSC Adv. 6 (2016) 23134–23140. https://doi.org/10.1039/c5ra26761g

[28] G. Liu, C. Sun, X. Yan, L. Cheng, Z. Chen, X. Wang, L. Wang, S.C. Smith, G.Q.

Lu, H.M. Cheng, Iodine doped anatase TiO_2 photocatalyst with ultra-long visible light response: Correlation between geometric/electronic structures and mechanisms, J. Mater. Chem. 19 (2009) 2822–2829. https://doi.org/10.1039/b820816f.

[29] H. Eskandarloo, A. Badiei, M.A. Behnajady, Optimization of UV/inorganic oxidants system efficiency for photooxidative removal of an azo textile dye, Desalin. Water Treat. 55 (2015) 210–226. https://doi.org/10.1080/19443994.2014.912965

[30] A. Mishra, B.S. Butola, Silver-Doped TiO_2 -Coated Cotton Fabric as an Effective Photocatalytic System for Dye Decolorization in UV and Visible Light, Photochem. Photobiol. 95 (2019) 522–531. https://doi.org/10.1111/php.13009

[31] C.H. Yu, C.H. Wu, T.H. Ho, P.K. Andy Hong, Decolorization of C.I. Reactive Black 5 in UV/TiO_2, UV/oxidant and UV/TiO_2/oxidant systems: A comparative study, Chem. Eng. J. 158 (2010) 578–583. https://doi.org/10.1016/j.cej.2010.02.001

[32] J. Hwang, S.S. Kalanur, H. Seo, Identification of Visible Photocatalytic and Photoelectrochemical Properties of I-TiO_2 via Electronic Band Structure, Electrochim. Acta 252 (2017) 482–489. https://doi.org/10.1016/j.electacta.2017.09.022

[33] V. Štengl, T.M. Grygar, The simplest way to iodine-doped anatase for photocatalysts activated by visible light, Int. J. Photoenergy 2011 (2011). https://doi.org/10.1155/2011/685935

[34] S.A. Alim, T.S. Rao, S.R. Miditana, K.V.D. Lakshmi, Efficient and recyclable visible light-active nickel–phosphorus co-doped TiO_2 nanocatalysts for the abatement of methylene blue dye, J. Nanostructure Chem. 10 (2020) 211–226. https://doi.org/10.1007/s40097-020-00343-z

[35] S.Y. Lee, H.T. Do, J.H. Kim, Microplasma-assisted synthesis of TiO_2–Au hybrid nanoparticles and their photocatalytic mechanism for degradation of methylene blue dye under ultraviolet and visible light irradiation, Appl. Surf. Sci. 573 (2022) 151383. https://doi.org/10.1016/j.apsusc.2021.151383

[36] S. Vishwanathan, S. Laxmi, S. Nandan, S. Jayan, M. Lijo, S. Das, Effect of experimental parameters on photocatalytic degradation efficiency of TiO_2 nanoparticles synthesized by electrochemical method towards Rhodamine B dye solution under natural sunlight, Environ. Sci. Pollut. Res. 30 (2023) 8448–8463. https://doi.org/10.1007/s11356-022-18835-6

[37] M. Syahin Firdaus Aziz Zamri, N. Sapawe, Regeneration Studies of TiO_2 Photocatalyst for Degradation of Phenol in a Batch System, Mater. Today Proc. 19 (2019) 1327–1332. https://doi.org/10.1016/j.matpr.2019.11.145

[38] M. Huang, C. Xu, Z. Wu, Y. Huang, J. Lin, J. Wu, Photocatalytic discolorization of methyl orange solution by Pt modified TiO_2 loaded on natural zeolite, Dye. Pigment. 77 (2008) 327–334. https://doi.org/10.1016/j.dyepig.2007.01.026

[39] Y. Chen, L. Feng, H. Li, Y. Wang, G. Chen, Q. Zhang, Biodegradation and detoxification of Direct Black G textile dye by a newly isolated thermophilic microflora, Bioresour. Technol. 250 (2018) 650–657. https://doi.org/10.1016/j.biortech.2017.11.092